Diffusion of myelin oligodendrocyte glycoprotein in living OLN-93 cells investigated by raster-scanning image correlation spectroscopy (RICS)
Non Peer-reviewed author version

Diffusion of myelin oligodendrocyte glycoprotein in living OLN-93 cells investigated by raster-scanning image correlation spectroscopy (RICS)

Ellen Gielen,[1,2,¥] Nick Smisdom,[2,¥] Ben De Clercq,[2,3] Martin vandeVen,[2] Rik Gijsbers,[4] Zeger Debyser,[4] Jean-Michel Rigo,[2] Johan Hofkens,[5] Yves Engelborghs,[1] Marcel Ameloot[2*]

(1) Laboratory for Biomolecular Dynamics, Catholic University Leuven, Celestijnenlaan 200G, B-3001 Heverlee, Belgium

(2) Laboratory for Cell Physiology, Biomedical Research Institute, Hasselt University and transnationale Universiteit Limburg, Agoralaan, Bldg D, B-3590 Diepenbeek, Belgium

(3) Department of Applied Physics, Eindhoven University of Technology, Den Dolech 2, P.O.Box 513, 5600 MB Eindhoven, The Netherlands

(4) Laboratory for Molecular Virology and Gene Therapy, Catholic University Leuven, Kapucijnenvoer 33 block i, B-3000 Leuven, Belgium

(5) Laboratory of Photochemistry and Spectroscopy, Catholic University Leuven, Celestijnenlaan 200F, B-3001 Heverlee, Belgium

Running head: Myelin-specific protein diffusion studied by means of RICS

 *Correspondence to: Marcel Ameloot, Hasselt University, Biomedical Research Institute, Laboratory of Cell Physiology, Agoralaan, Bldg D, B-3590 Diepenbeek, Belgium

Tel.: 00-32-11-26.85.46

Fax: 00-32-11-26.85.99

E-mail: marcel.ameloot@uhasselt.be

¥ Ellen Gielen and Nick Smisdom contributed equally to this work

ABSTRACT

Many membrane proteins and lipids are partially confined in substructures ranging from tens of nanometers to micrometers in size. Evidence for heterogeneities in the membrane of oligodendrocytes, i.e. the myelin-producing cells of the central nervous system, is almost exclusively based on detergent methods. However, as application of detergents can alter the membrane phase behaviour, it is important to investigate membrane heterogeneities in living cells. Here, we report on the first investigations of the diffusion behavior of the myelin-specific protein MOG (myelin oligodendrocyte glycoprotein) in OLN-93 as studied by the recently developed RICS (raster-scanning image correlation spectroscopy) technique. We implemented RICS on a standard confocal laser-scanning microscope with one-photon excitation and analog detection. Measurements on FITC-dextran were used to evaluate the performance of the system and the data analysis procedure.

INTRODUCTION

The plasma membrane of various mammalian cell types is heterogeneous in structure and may contain microdomains, which can impose constraints on the lateral diffusion of its constituents. One type of membrane inhomogeneities consists of the so-called lipid rafts, built mainly of cholesterol and saturated lipids [1]. These liquid-ordered microdomains attract a lot of interest as they are thought to provide dynamic platforms that are involved in a variety of processes, such as signal transduction and protein and lipid sorting [2].

Oligodendrocytes (OLGs) are the myelin-producing cells of the central nervous system. Mature OLGs provide the ensheathment of axons with myelin, which is essential for the fast saltatory conduction of action potentials. Abnormalities in myelin development or disturbance and destruction of its structure lead to severe neurological symptoms observed in diseases such as multiple sclerosis (MS) [3-5]. Maintenance of the functional myelin sheath requires a carefully regulated balance of myelin synthesis and turnover, requiring precise sorting and targeting mechanisms. The formation of lipid rafts in OLGs may be important for membrane subdomain organization, compartmentalization of signalling molecules and sorting of myelin components [6].

Most of the experimental evidence concerning the membrane heterogeneity in oligodendroglial membranes is based on biochemical studies [6], which show that some membrane constituents are resistant to solubilization by nonionic detergents at low temperature [7]. The amount of proteins and lipids, however, as well as the sucrose gradient buoyancy of the detergent-resistant membrane complexes, was reported to vary substantially among the detergents and extraction procedure used [8-9]. Application of a detergent alters the membrane phase behavior [10-11]. In

addition, the exact relationship between rafts and detergent-resistant membranes is unclear [12]. Therefore, it is important to investigate actual membrane heterogeneities in living OLGs. This can be accomplished by using microfluorimetric methods for monitoring the diffusion of molecules in the plane of the membrane [13].

One method that can be used to investigate the dynamic properties of molecules diffusing in the plasma membrane of living cells is fluorescence correlation spectroscopy (FCS) in its various modalities. In FCS small fluctuations in the fluorescence signal from a femtoliter stationary or scanned observation volume are measured over a short period of time [14-15]. These fluctuations arise from fluorescently labeled molecules diffusing in and out of this observation volume, which is spatially defined by the laser focus. The corresponding autocorrelation function (ACF) contains information about the average number of molecules in the observation volume (N) and their characteristic diffusion time [16]. Recently we have been able to demonstrate using Z-scan FCS that the lipid probe DiD (1,1'-dioctadecyl-3,3,3',3'-tetramethylindodicarbocyanine perchlorate) exhibits hindered diffusive motion in the plasma membrane of the OLN-93 oligodendroglial cell line [17]. In the current work we elaborate on the mobility of the transmembrane protein MOG (myelin oligodendrocyte glycoprotein) in living OLN-93 cells.

MOG is an integral myelin-specific protein, which is localized in the outer lamella of the myelin sheath and therefore exposed to the extracellular environment. Although MOG is only a minor component of the myelin membrane (0.01-0.05 % of the total myelin protein content), it induces severe experimental autoimmune encephalitis, i.e. the animal model of MS, after administration to both rodents and primates [18-19]. Furthermore, injection of monoclonal antibodies against MOG into rodents causes extensive myelin destruction *in situ* [20]. The association of MOG

with Triton X-100 insoluble lipids is thought to activate signalling pathways related to stress response and cytoskeletal instability, inducing the retraction of OLG processes [21-22] and thus demyelination.

In this work, control measurements on FITC-dextran (fluorescein isothiocyanate-dextran) were performed to validate the RICS (raster-scanning image correlation spectroscopy) method and the in-house software for data analysis. RICS was then applied to monitor the diffusion of MOG in a stable OLN-93 oligodendroglial cell line [23] expressing MOG-eGFP (enhanced green fluorescent protein, with eGFP linked to the intracellular C-terminus of MOG).

THEORETICAL BACKGROUND

RICS has been introduced by Digman et al. [24-25] and the principles are briefly reiterated here for the convenience of the reader. RICS operates on a temporal series of images obtained with a laser-scanning microscope (raster-scan mode). Each raster-scan image in this series contains temporal information as it is formed pixel by pixel and line by line (Fig. 1A). Adjacent pixels along a single (horizontal) line are a few microseconds (pixel dwell time, τ_p) apart, while pixels over successive (vertical) lines and frames are respectively a few milliseconds (line time, τ_l) and seconds-to-minutes apart. Hence, the spatial correlation of the image yields information on molecular dynamics over a broad time window. RICS allows combination of the temporal scales of single-point FCS with the spatial information obtained from ICS (image correlation spectroscopy) [26-27].

The overall normalized two-dimensional fluorescence intensity fluctuation spatial ACF ($G_S(\xi,\psi)$) is defined as:

$$G_S(\xi,\psi) = \frac{\langle \delta I(x,y)\delta I(x+\xi, y+\psi)\rangle_{x,y}}{\langle I(x,y)\rangle^2_{x,y}} = G(\xi,\psi)\ S(\xi,\psi) \qquad (1)$$

where I(x,y) is the detected fluorescence intensity at each pixel and δI(x,y) = I(x,y) - <I(x,y)> are the fluorescence intensity fluctuations around the mean intensity of the image <I(x,y)>.

The transition from FCS to RICS is made by defining a scan function that relates time with space:

$$\tau(\xi,\psi) = \tau_p\xi + \tau_l\psi \qquad (2)$$

where ξ and ψ are the spatial displacements, expressed in number of pixels, in the x (pixels along a line) and y (pixels in successive lines) direction in the raster image, respectively (Fig. 1B). The ACF for 3D diffusion then becomes (for one-photon excitation):

$$G(\xi,\psi) = \frac{\gamma}{N}\left(1 + \frac{4D(\tau_p\xi + \tau_l\psi)}{\omega_0^2}\right)^{-1}\left(1 + \frac{4D(\tau_p\xi + \tau_l\psi)}{\omega_z^2}\right)^{-1/2} \qquad (3)$$

For diffusion in a plane the last factor in Eq. (3) must be omitted. The factor γ accounts for the non-uniform illumination of the excitation volume and is equal to 0.3535 for a 3D [28] and 0.5 for a 2D Gaussian point spread function (PSF). $G(\xi,\psi)$ is the ACF due to molecular diffusion only. Since the PSF overlaps several pixels in the xy-plane (requisite for RICS), there also is a correlation due to the scanning itself. For square pixels with dimension $\delta r \times \delta r$ this correlation $(S(\xi,\psi))$ is given by:

$$S(\xi,\psi) = \exp\left(-\frac{\left[\left(\frac{\xi\delta r}{\omega_0}\right)^2 + \left(\frac{\psi\delta r}{\omega_0}\right)^2\right]}{1 + \frac{4D(\tau_p\xi + \tau_l\psi)}{\omega_0^2}}\right) \tag{4}$$

It is clear from Eq. (3) that the spatial ACF in RICS behaves in approximately the same way as the temporal ACF in FCS. As for FCS, the amplitude of the spatial autocorrelation curve is inversely proportional to the particle concentration [29]. In addition, the correlation curve will broaden when the diffusion becomes slower. One of the main advantages of RICS over FCS is that kinetic information can be spatially mapped allowing for the detection of heterogeneities in diffusion [24].

MATERIALS AND METHODS

Chemicals

FITC-dextran with a molecular weight of 2000 kDa (FD2000S) and a hydrodynamic radius of 32.8 nm [30] was purchased from Sigma-Aldrich NV (Bornem, Belgium). Dilutions of FD2000S were made in Tris buffer pH 10 and in HEPES-buffered medium without phenol red (MWPR; Gibco BRL, supplied by Invitrogen, Merelbeke, Belgium), respectively. To perform RICS measurements, the fluorescent solutions were "sandwiched" between a microscope slide and a coverslip, sealed by an adhesive spacer of 120 μm thickness in between (Secure-seal spacer, Molecular Probes, supplied by Invitrogen). The generated microscopic chamber is small enough to eliminate any flow or currents in the solution while retaining a 3D sample environment [31]. Measurements were performed at 28°C (Tris buffer pH 10), respectively 23°C (MWPR).

Cell culture

The OLN-93 cell line was kindly provided by Prof. Dr. Christiane Richter-Landsberg (University of Oldenburg, Germany). A stable MOG-eGFP-expressing OLN-93 cell line was generated by means of lentiviral vector technology. The cell line was further modified into a stable galactosylceramide and sulfatide-expressing (GS) MOG-eGFP OLN-93 cell line by Dr. Wia Baron (lab of Prof. Dr. Dick Hoekstra; laboratory for membrane cell biology, University Medical Centre Groningen, University of Groningen, The Netherlands). OLN-93 GS cells expressing MOG-eGFP were cultured on 24 mm ∅ coverslips in DMEM (Gibco BRL, cat. no. 41965-039) supplemented with 10% foetal bovine serum (Sigma-Aldrich), 100 U/ml penicillin,

100 µg/ml streptomycin (Gibco BRL), 1 µg/ml puromycin and 2 mg/ml geneticin (Sigma-Aldrich) in a humidified 10% CO_2 incubator at 37°C. For RICS measurements, cells were mounted in a homemade bath chamber and the cell culture medium was replaced by MWPR. Measurements were performed at the membrane facing the glass coverslip. For fixation, cells were put in 4% paraformaldehyde (PFA) at 4°C. After 10 min of incubation, PFA was replaced by MWPR.

Viscosity Determination

The viscosities of TRIS buffer pH 10 and MWPR were determined with a model AR G-2 rheometer (Tain Instruments Corp., div. of Waters NV/SA, Zellik, Belgium) at various temperatures (23°C and 28°C). The instrument was calibrated before every measurement and care was taken to avoid the introduction of air bubbles. Each sample (1 ml, filtered through a 0.22 µm Sterivex filter, Millipore Corporation, supplied by VWR International Europe BVBA, Leuven, Belgium) was allowed to equilibrate for at least 10 minutes before measurements were started.

Instrumental set-up

RICS images were collected with a Zeiss LSM 510 META one-photon confocal laser-scanning microscope (Jena, Germany) on an Axiovert200M motorized frame. An analog photomultiplier tube (proprietary Zeiss information) was used for detection. Samples were excited with the 488 nm line (selected by a 488 ± 10 nm interference-based laser cleanup filter) of the 20 mW air-cooled argon ion laser (set at 70% of its maximum power) under the control of an AOTF (set at 1% transmission; ~ 10 µW at the sample position). The excitation light was directed to the sample via a dichroic

mirror (DC; HFT 488) and a Zeiss EC Plan-Neofluar 40x/NA 1.3 oil immersion objective. The fluorescence light was directed through the DC and a LP505 emission filter to the photomultiplier detector. The pinhole size was 1 Airy unit. Images were collected using the 4.0 version of the Zeiss software. The image size was typically set to 512×512 pixels and the zoom factor to 8 (54.9 nm/pixel) to ensure that the PSF contained a sufficiently large number of pixels (radius of 5-6 pixels). The $1/e^2$ axial ($\omega_z = 1.8$ µm) and lateral ($\omega_0 = 0.31$ µm) waists of the PSF were determined by performing a z-stack on 175 nm fluorescent beads (Molecular Probes, PS-Speck microscope point source Kit, yellow-green fluorescent 505/515) and by fitting the obtained intensity profiles in xy-direction and in z-direction with a Gaussian profile.

Fluorescence recovery after photobleaching (FRAP) experiments were performed on the same set-up using a bleaching pulse at maximum intensity for 150.6 ms yielding a bleaching depth of 40 %. The diameter of the bleached area was 50 pixels (= 2.75 µm).

All measurements were performed at room temperature (23°C) to minimize cell movement.

Data analysis

Data were analysed with the RICS software from the Laboratory of Fluorescence Dynamics (E. Gratton, Irivine) and an in-house program in a Matlab environment (MatlabR2007a version 7.4, The MathWorks, Gouda, The Netherlands) incorporating routines as made available by Kolin and described by Costantino et al. (2005) [32]. Simulations were run in this program to determine the optimal scan speed for recovery of the diffusion coefficient. The parameters of the models were estimated by

weighted least squares, with weights calculated from the standard deviations (σ) of the set of autocorrelation functions determined from the images of the series.

Analysis of FRAP experiments was performed according to Soumpasis [33]. A control region was collected simultaneously with the bleached area to correct for readout bleaching.

Uncertainties are reported as standard deviations.

RESULTS

3D diffusion measurements in isotropic solution

Fig. 2 shows the autocorrelation spectrum for FD2000S diffusing freely in Tris buffer pH 10, after subtraction of the background (scan speed 9: τ_p = 1.6 µs/pixel; series with 100 images). Due to the rather high scan speed, the correlated detector noise is clearly visible in the spectrum. By omitting any influence of (un)correlated noise, the quality and accuracy of the fit is optimal. The ψ = 0 line was therefore omitted. Cropping the autocorrelation spectrum to a 16×16 region and fitting with a 3D free diffusion model yields a diffusion coefficient D = 8.5 ± 0.2 µm^2/s. Very similar values were obtained by varying crop size. It is clear, by comparing the measured spectrum with the fitted spectrum, that the effective value of G(0,0) is lower than the noise-containing spectrum might suggest. Measurements performed in MWPR yield a diffusion coefficient D = 6.7 ± 0.4 µm^2/s. Parameter values are summarized in Table I.

2D diffusion measurements in cell membrane

A scanned image (scan speed 2: τ_p = 102.4 µs/pixel) of a single OLN-93 GS cell expressing MOG-eGFP is shown in Fig. 3A. The image series contained 65 images. The regions of interest (ROIs) for RICS analysis were selected on the basis of apparent homogeneity and were taken at some distance from the cell borders. Seven 64x64 ROIs with a relative horizontal shift of 32 pixels were analyzed for simple 2D diffusion. For clarity, only four of the seven ROIs are shown in Fig. 3A. The average diffusion coefficient is 0.10 ± 0.01 µm^2/s. Fig. 3C and 3D show the fitted spectrum and corresponding residuals for ROI 3 depicted in Fig. 3A.

A set of three FRAP experiments using a bleached area with a diameter of 50 pixels (= 2.75 μm) yielded an average diffusion coefficient D = 0.19 ± 0.04 μm^2/s. The immobile fraction was 0.67 ± 0.12.

Negative control experiments were performed on fixed cells. The value of the diffusion coefficient recovered by FRAP experiments was on the order of 2x10^{-4} μm^2/s. In the RICS experiments (scan speed 2, 75 images), various 64x64 regions were considered and formally analyzed for 2D diffusion. The values for the diffusion coefficients at convergence during the least squares search exhibited very strong dependence on the initial guess. The sum of the weighted squared residuals (SWSR) is within a very broad range essentially independent on the value of the diffusion coefficient when fixed in the analysis and equals the value of the SWSR obtained when the diffusion coefficient is fixed to zero. This is in contrast with the dependence of the SWSR on the value of the diffusion coefficient when fixed in the analysis of the RICS data obtained on living cells. A similar pattern was found for analyses of corresponding simulations.

DISCUSSION AND CONCLUSIONS

RICS is a non-invasive fluorimetric technique that can be performed on any standard laser-scanning microscope. We implemented RICS on a Zeiss LSM510 META confocal laser-scanning microscope with one-photon excitation and analog detection. Control measurements on FD2000S in isotropic solution were performed to validate the method and the in-house software for data analysis. Table I shows that the measured and expected (Stokes-Einstein) values for the diffusion coefficient are quite similar.

RICS characterization of the 2D membrane diffusion of MOG-eGFP yields values for the diffusion coefficient in agreement with values reported for other transmembrane proteins [34-37]. The average value of the diffusion coefficient is of the same order as the value obtained with FRAP. However, comparison between FRAP and RICS results cannot directly be made, even when the region of interest is of comparable size. In a FRAP experiment, the mobility of the fluorescent molecules in the non-bleached area is indirectly sampled as well, so that the recovered diffusion coefficient is an average over a much wider area than the bleached spot. The value of the diffusion coefficient obtained in RICS is more locally defined. RICS is more appropriate for detecting different molecular mobilities in spatially different areas of the cell membrane. This allows for mapping of the diffusion coefficient over the cell membrane. The current implementation of RICS does not allow for determination of immobile fractions. According to our knowledge, this is the first time that RICS has been applied to study the membrane diffusion in living oligodendroglial cells.

So far, we have only considered simple 2D diffusion models. Future experiments will be designed in order to find out about possible hindered diffusion of MOG-eGFP in the plasma membrane of OLN-93 GS cells. Measurements at 37°C and spatial mapping of diffusion coefficients over the cell surface under varying conditions (e.g. cholesterol depletion) are in progress. Further studies will comprise the inherent dimerization properties of the MOG molecule [38] and the possible interference of the eGFP moieties [39] on this will be explored.

ACKNOWLEDGEMENTS

REFERENCE LIST

1. A. Kusumi, I. Koyama-Honda, and K. Suzuki, (2004), Molecular dynamics and interactions for creation of stimulation-induced stabilized rafts from small unstable steady-state rafts, Traffic 5(4), 213-230.

2. K. Simons, and E. Ikonen, (1997), Functional rafts in cell membranes, Nature 387(6633), 569-572.

3. P.F. Bartlett, and I.R. Mackay, (1983), The oligodendroglial cell: biology and immunology and relationship to multiple sclerosis, J. Clin. Lab. Immunol. 11(1), 1-7.

4. N. Baumann, and D. Pham-Dinh, (2001), Biology of oligodendrocyte and myelin in the mammalian central nervous system, Physiol Rev. 81(2), 871-927.

5. H. de Vries, and D. Hoekstra, (2000), On the biogenesis of the myelin sheath: cognate polarized trafficking pathways in oligodendrocytes, Glycoconj.J. 17(3-4), 181-190.

6. E. Gielen, W. Baron, M. vandeVen, P. Steels, D. Hoekstra, and M. Ameloot, (2006), Rafts in oligodendrocytes: evidence and structure-function relationship, Glia 54(6), 499-512.

7. D.A. Brown, and J.K. Rose, (1992), Sorting of GPI-anchored proteins to glycolipid-enriched membrane subdomains during transport to the apical cell surface, Cell 68(3), 533-544.

8. L.S. DeBruin, J.D. Haines, L.A. Wellhauser, G. Radeva, V. Schonmann, D. Bienzle, and G. Harauz, (2005), Developmental partitioning of myelin basic protein into

membrane microdomains, J Neurosci Res 80(2), 211-225.

9. C.M. Taylor, T. Coetzee, and S.E. Pfeiffer, (2002), Detergent-insoluble glycosphingolipid/cholesterol microdomains of the myelin membrane, J Neurochem 81(5): 993-1004.

10. H. Heerklotz, (2002), Triton promotes domain formation in lipid raft mixtures, Biophys J 83(5), 2693-2701.

11. H. Heerklotz, H. Szadkowska, T. Anderson, and J. Seelig, (2003), The sensitivity of lipid domains to small perturbations demonstrated by the effect of Triton, J Mol Biol 329(4), 793-799.

12. H. Shogomori, and D.A. Brown, (2003), Use of detergents to study membrane rafts: the good, the bad, and the ugly, Biol Chem 384(9), 1259-1263.

13. D. Marguet, P.F. Lenne, H. Rigneault, and H.T. He, (2006), Dynamics in the plasma membrane: how to combine fluidity and order, EMBO J 25(15), 3446-3457.

14. R. Rigler, and E.S. Elson (2001) Fluorescence Correlation Spectroscopy: Theory and Applications, Springer, New York.

15. K. Bacia, and P. Schwille, (2003), A dynamic view of cellular processes by in vivo fluorescence auto- and cross-correlation spectroscopy, Methods 29(1), 74-85.

16. E. Haustein, and P. Schwille, (2004), Single-molecule spectroscopic methods, Curr Opin Struct Biol 14(5), 531-540.

17. J. Humpolikova, E. Gielen, A. Benda, V. Fagulova, J. Vercammen, M. vandeVen, M. Hof, M. Ameloot, and Y. Engelborghs, (2006), Probing diffusion laws within cellular membranes by Z-scan fluorescence correlation spectroscopy, Biophys J

91(3), L23-25.

18. A. Iglesias, J. Bauer, T. Litzenburger, A. Schubart, and C. Linington, (2001), T- and B-cell responses to myelin oligodendrocyte glycoprotein in experimental autoimmune encephalomyelitis and multiple sclerosis, Glia 36(2), 220-234.

19. T.G. Johns, and C.C. Bernard, (1999), The structure and function of myelin oligodendrocyte glycoprotein, J Neurochem 72(1), 1-9.

20. C. Linington, M. Bradl, H. Lassmann, C. Brunner, and K. Vass, (1988), Augmentation of demyelination in rat acute allergic encephalomyelitis by circulating mouse monoclonal antibodies directed against a myelin/oligodendrocyte glycoprotein, Am J Pathol 130(3), 443-454.

21. C.B. Marta, C.M. Taylor, T. Coetzee, T. Kim, S. Winkler, R. Bansal, and S.E. Pfeiffer, (2003), Antibody cross-linking of myelin oligodendrocyte glycoprotein leads to its rapid repartitioning into detergent-insoluble fractions, and altered protein phosphorylation and cell morphology, J Neurosci 23(13), 5461-5471.

22. C.B. Marta, M.B. Montano, C.M. Taylor, A.L. Taylor, R. Bansal, and S.E. Pfeiffer, (2005), Signaling cascades activated upon antibody cross-linking of myelin oligodendrocyte glycoprotein: potential implications for multiple sclerosis, J Biol Chem 280(10), 8985-8993.

23. C. Richter-Landsberg, and M. Heinrich, (1996), OLN-93: a new permanent oligodendroglia cell line derived from primary rat brain glial cultures, J Neurosci Res 45(2), 161-173.

24. M.A. Digman, C.M. Brown, P. Sengupta, P.W. Wiseman, A.R. Horwitz, and E. Gratton, (2005), Measuring fast dynamics in solutions and cells with a laser

scanning microscope, Biophys J 89(2), 1317-1327.

25. M.A. Digman, P. Sengupta, P.W. Wiseman, C.M. Brown, A.R. Horwitz, and E. Gratton, (2005), Fluctuation correlation spectroscopy with a laser-scanning microscope: exploiting the hidden time structure, Biophys J 88(5), L33-36.

26. N.O. Petersen, P.L. Hoddelius, P.W. Wiseman, O. Seger, and K.E. Magnusson, (1993), Quantitation of membrane receptor distributions by image correlation spectroscopy: concept and application, Biophys J 65(3), 1135-1146.

27. B. Hebert, S. Costantino, and P.W. Wiseman, (2005), Spatiotemporal image correlation spectroscopy (STICS) theory, verification, and application to protein velocity mapping in living CHO cells, Biophys J 88(5), 3601-3614.

28. B.K. Muller, E. Zaychikov, C. Brauchle, and D.C. Lamb, (2005), Pulsed interleaved excitation, Biophys J 89(5), 3508-3522.

29. N.O. Petersen, (1986), Scanning fluorescence correlation spectroscopy. I. Theory and simulation of aggregation measurements, Biophys J 49(4), 809-815.

30. K. Braeckmans, L. Peeters, N.N. Sanders, S.C. De Smedt, and J. Demeester, (2003), Three-dimensional fluorescence recovery after photobleaching with the confocal scanning laser microscope, Biophys J 85(4), 2240-2252.

31. K. Braeckmans, K. Remaut, R.E. Vandenbroucke, B. Lucas, S.C. De Smedt, and J. Demeester, (2007), Line FRAP with the confocal laser scanning microscope for diffusion measurements in small regions of 3-D samples, Biophys J 92(6), 2172-2183.

32. S. Costantino, S.J.W. Comeau, D.L. Kolin, and P.W. Wiseman, (2005), Accuracy and dynamic range of spatial image correlation and

cross-correlation spectroscopy, Biophys J 89(2), 1251-1260. (http://wiseman-group.mcgill.ca/colin.php)

33. D.M. Soumpasis, (1983), Theoretical analysis of fluorescence photobleaching recovery experiments, Biophys J 41(1): 95-97.

34. W.W. Webb, L.S. Barak, D.W. Tank, and E.S. Wu, (1981), Molecular mobility on the cell surface, Biochem Soc Symp (46), 191-205.

35. M. Srivastava, and N.O. Petersen, (1998), Diffusion of transferrin receptor clusters, Biophys Chem 75(3), 201-211.

36. P.W. Wiseman, J.A. Squier, M.H. Ellisman, and K.R. Wilson, (2000), Two-photon image correlation spectroscopy and image cross-correlation spectroscopy, J Microsc 200(Pt1), 14-25.

37. A.K. Kenworthy, B.J. Nichols, C.L. Remmert, G.M. Hendrix, M. Kumar, J. Zimmerberg, and J. Lippincott-Schwartz, (2004), Dynamics of putative raft-associated proteins at the cell surface, J Cell Biol 165(5), 735-746.

38. P. Hjelsmström, J.E. Penzotti, R.M. Henne, and T.P. Lybrand, (1998), A molecular model of myelin oligodendrocyte glycoprotein, J Neurochem 71, 1742-1749.

39. R.Y. Tsien, (1998), The green fluorescent protein, Annu Rev Biochem 67: 509- 544.

FIGURE LEGENDS

Figure 1 (A) Raster-scan images contain temporal information because pixels are recorded sequentially. Note that RICS analysis requires oversampling of the PSF, i.e. δr has to be substantially smaller than the width of the PSF. (B) Graphical representation of the 2D spatial correlation of a raster-scan image obtained by shifting a duplicate of the picture (depicted in dashed lines) over ξ and ψ, respectively, the horizontal and vertical directions. The corresponding mathematical expression is given in Eq. (4).

Figure 2 (A) Measured correlation spectrum (truncated along the $G_S(\xi,\psi)$ axis for display purposes); (B) standard deviation plot; (C) fitted correlation spectrum (3D free diffusion model) and (D) corresponding weighted residuals of FD2000S diffusing freely in TRIS buffer pH 10. 100 images were collected at scan speed 9. τ_p = 1.6 µs/pixel; τ_l = 1.92 ms; T = 28°C. Parameter values are summarized in Table I.

Figure 3 (A) Fluorescence image of a single OLN-93 MOG-eGFP GS cell; (B) standard deviation plot; (C) fitted autocorrelation curve (2D free diffusion model) and (D) corresponding weighted residuals of ROI 3 (64x64 pixels; total area of 12.4 µm²) depicted in (A). 65 images were collected at scan speed 2. τ_p = 102.4 µs/pixel; τ_l = 122.9 ms; T = 23°C.

FIGURES

Figure 1

A Correlation spectrum

B Standard deviation

C Fitted correlation spectrum

D Weighted residuals

Figure 2

A

B Standard deviation

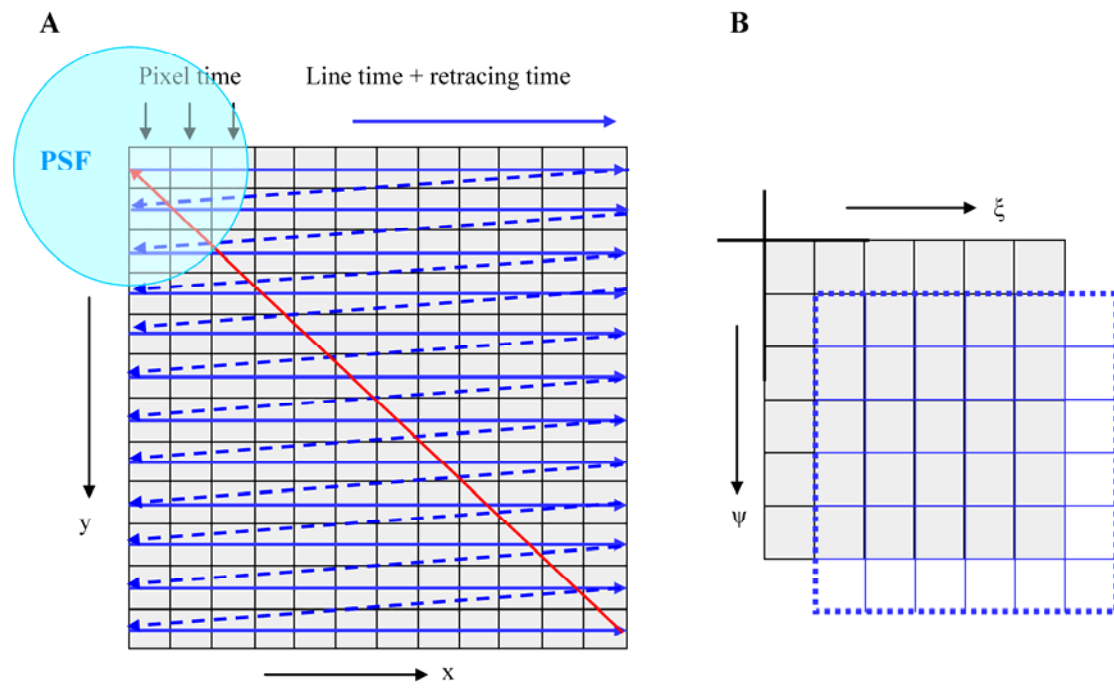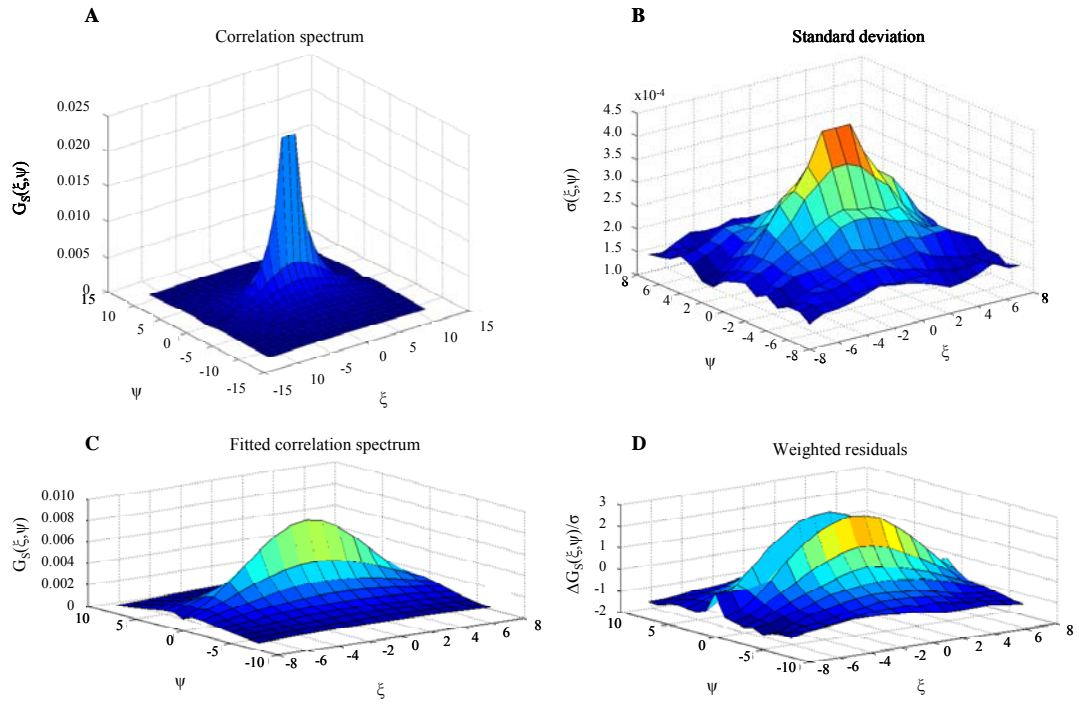**C** Fitted correlation spectrum
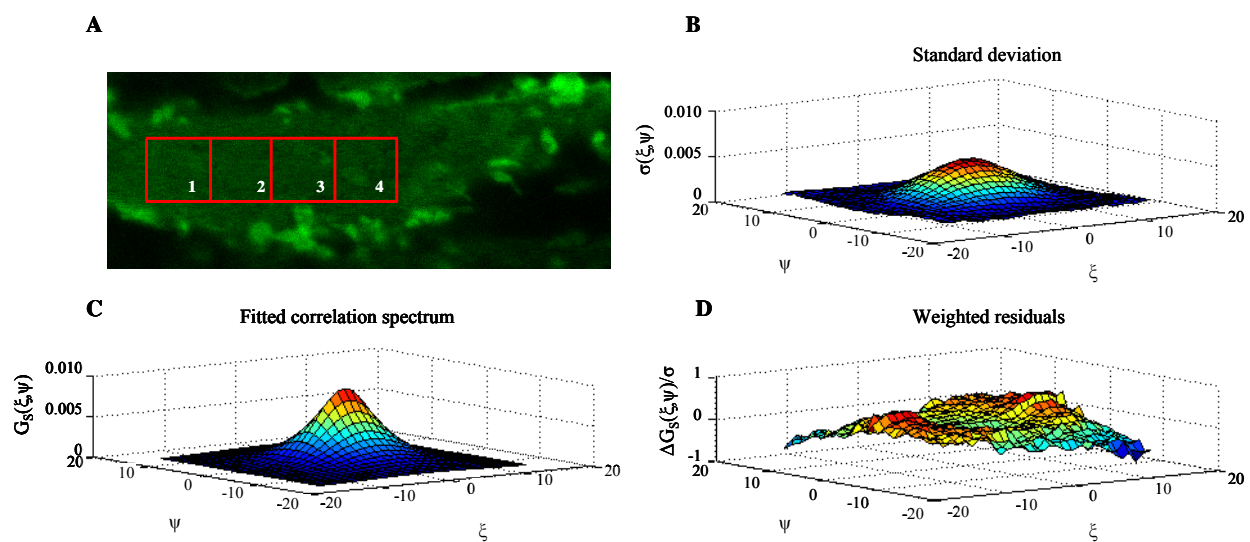
D Weighted residuals

Figure 3

Table I Summary of 3D diffusion measurements on FD2000S in isotropic solution

Solution	Viscosity (mPa.s)	T (°C)	τ_p (µs)	τ_l (ms)	D (µm²/s)	$D_{expected}$ (Stokes-Einstein) (µm²/s)
Tris buffer	0.78	28	0.91	1.09	8.5 ± 0.2*	8.6
MWPR	0.92	23	0.91	1.09	6.7 ± 0.4*	7.2

*Uncertainties are reported as standard deviations.